Self-consistent 3D fluid modelling of the interaction between flushed and reciprocating probes and a turbulent Scrape-Off-Layer

R. Futtersack[1]*, **P. Tamain**[1], **G. Ciraolo**[1], **C. Colin**[2], **N. Fedorczak**[1], **Ph. Ghendrih**[1], **Y. Marandet**[3], **F. Schwander**[2], et **E. Serre**[2]

[1] CEA-IRFM, F-13108 Saint-Paul-lez-Durance, France
[2] Aix-Marseille Université, CNRS, Centrale Marseille, M2P2 UMR 7340, 13451 Marseille, France
[3] Aix-Marseille Université, CNRS, PIIM, UMR 7345, Marseille F-13397, France

Received XXXX, revised XXXX, accepted XXXX
Published online XXXX

Key words Langmuir, probes, plasma, turbulence, SOL, 3D

3D interplay between Langmuir probes (LP) and Scrape-Off-Layer (SOL) plasma turbulence is numerically investigated with the TOKAM3X fluid code. A flushed LP is modelled by biasing a part of the target plates surface. The probe is found to drive a polarization of the plasma and consequently to impact the transverse transport. The perturbation extends along the connected flux tube, and, depending on both the length of the field lines and the plasma collisionnality, can reach the next solid obstacle and draw current from it. The characteristics of the SOL turbulent plasma in the shadow of a probe body are also heavily impacted. In consequence, synthetic Mach measurements differ significantly from one can expect of the classical Hutchinson theory.

1 Introduction

Scrape-Off-Layer turbulence studies mostly relie on plasma fluctuations measurements by the means of Langmuir probes (LP) [1–8]. Despite their apparent simplicity, probes comes with an historitical and rather complex theory: first measurements of IV characteristics were initated in 1923 by Langmuir [1] and after few years, he provided the bases of the *quasineutral* plasma-sheath theory [2,3]. Some decades later, Bohm describes the effect of magnetic field on electrical probes and suggests his famous Bohm criterion [4]. A large body of litterature follow then, attemting to build a reliable theory on probe measuremens : describing ion collection physics [9–15], kinetic effects [16, 17] of electrons and perturbations due to polarization [18–23].

OML [24]

ABR [25]

BRL [26, 27]

As the subject of LP measurements theory and induced perturbations of the plasma is substantial and complex, this paper aims only at looking the perturbations caused by the probe on transport properties. Previous studies , modelling this probe-plasma interaction by biasing the target plates in the 2D interchange code TOKAM2D, showed that the presence of a LP in ion saturation mode significantly disturbs the plasma. In fact, as in biasing experiments [20], the polarization of the flux tube connected to the LP leads to the formation of a convective cell, which acts then as a transport barrier preventing the turbulent plasma to reach the probe tip. Here, we look at the effect of the parallel dynamics on the perturbation, and we study for the first time the impact on the turbulent plasma of the immersion of an object into the SOL.

Whilst the ion collection theory has been built up over a long history, current transport induced by a biased probe has been largely forsaken. Yet, some experimental evidences published by Matthews, Pitts and Stangeby [13, 18, 19] show with the pin-plate probe that when a surface is polarized negatively with respect to the wall of the device,

* Corresponding author E-mail: romain.futtersack@gmail.com, Phone: +33 630 718 763

Analysis of the probe characteristics includes the pattern of the current short-circuiting in the ambient plasma in front the probe as well as determination of the sizes of the return current collecting zone on the divertor plates. Such an analysis depends crucially on the type of effective conductivity perpendicular to the magnetic field.

If the saturation currents drawn by the probe are directly dependents of the probe surface increased by the sheath expansion. The shape of the IV carac is fundamentaly linked to the surface of the return current. If no transverse transport, the flux tube extends up to the first solid object and the return sheath collection area will be of approximately the same area as the probe collection area. If perp transport, some of the current will return around the probe

the probe circuit has to be completed through some sheath bounding the plasma. If the collection area of the return sheath is larger than the probe one, the probe theory is a good approximation

Mach Probes [9–13, 28] non local perturbation Paredes [29]

While all the previous studies and theories assumes an ad-hoc anomalous perpendicular transport, we intend here to look at the ion collection problem in a typical SOL turbulence context.

This paper is organized as follows. In section 2 we present the TOKAM3X code [30] and the modelling of the synthetic probes in a 3D-slab geometry. In section 3, we analyse the plasma perturbations caused by the biasing of a LP flushed in the divertor. In section 4, we look at the case of a mobile probe, unbiased, plunged into the SOL, and use our synthetic datas to reproduce Mach measurements. Section 5

2 Synthetic probe modelling in the TOKAM3X fluid code

The TOKAM3X code has been developped in the framework of a long-term program dedicated to edge transport modelling. TOKAM3X solves the drift-reduced Braginskii conservative equations in an arbitrary 3D magnetic geometry (from limited to multiple X-points). The model is able to describe the core and the SOL plasmas, without any scale separation between the size of the device and those of plasma fluctuations allowing the code to recover, in a self-consistent way, large scale flows as well as the characteristic SOL electrostatic turbulence.

2.1 Fluid model of the SOL turbulent transport

The SOL plasma consists of electrons following a Boltzmann distribution and a single ion specie of mass m_i and charge e. The plasma is assumed quasineutral which allows to solve the current conservation $\nabla \cdot \mathbf{j} = 0$ equation (in conjunction with the parallel Ohm's law) to recover the electrostatic potential. Perpendicular transport is described in term of drifts (electric, diamagnetic and polarization) assuming its characteristic frequency scale is small with respect to the ion gyro-frequency $\omega_c = eB/m_i$. Reference plasma density n_0 and temperature T_0 are then used to make dimensionless the fluid quantities and equations. The electrostatic potential Φ is normalized to T_0/e, velocities to a thermal speed $c_s = \sqrt{(eT_0/mi)}$, times to ω_c^{-1} and lenghts to $\rho_L = c_s\omega_c^{-1}$ accordingly. Temperature distribution of electrons T_e and ions T_i are chosen uniform and equal, eg. $T_e = T_i = 1$.

In this work, equations are solved in a simplified 3D slab geometry, with $X \equiv (r-a)/\rho_L$ and $Y \equiv r\theta/\rho_L$, both perpendicular to the magnetic field $\mathbf{B} = B_0\mathbf{b}$ (r and θ being the minor radius and the poloidal angle coordinates and a the minor radius at the separatrix). The parallel direction is indicated by $Z \equiv \varphi/\rho_L$. All curvature terms are dropped except the divergence of the diamagnetic current which drives the interchange instability [21].

Conservation equations of the model then read:

$$\partial_t N + \nabla \cdot (N\mathbf{u}_E) - D\nabla_\perp^2 N = S - \nabla \cdot \big(N(\Gamma_\parallel - J_\parallel)\mathbf{b}/N\big) \tag{1}$$

$$\partial_t \Gamma_\parallel + \nabla \cdot \big(\Gamma_\parallel \mathbf{u}_E\big) - D_\Gamma \nabla_\perp^2 \Gamma_\parallel = -2\nabla_\parallel N - \nabla \cdot \Big(\Gamma_\parallel^2 \mathbf{b}/N\Big) \tag{2}$$

$$J_\parallel = -\eta_\parallel^{-1} \nabla_\parallel \left(\Phi - \ln N\right) \tag{3}$$

$$\partial_t W + \nabla \cdot (W\mathbf{u}_E) - \nu\nabla_\perp^2 W = -g\nabla_y N + \nabla \cdot \big(J_\parallel \mathbf{b}\big) - \nabla \cdot \big(W\Gamma_\parallel \mathbf{b}/N\big) \tag{4}$$

The two first equations (1) and (2) correspond respectively to the conservation of electron density N and parallel ion momentum $\Gamma_\parallel$. Electron transport along magnetic field lines, neglecting inertia, leads to a parallel Ohm's law Eq. (3) relating the parallel current $J_\parallel$ to the parallel gradients of the potential and pressure. Eq. (4) derives

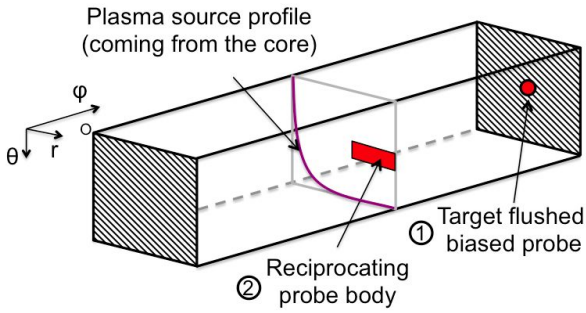

Fig. 1 Sketch of the slab geometry for the SOL. Divertor plates are located at the end of the field lines, depicted with hatchings. The flushed probe is situated in the center of the top divertor plate and the mobile probe inserted in the middle of the domain. The profile of the source term driving the system is aslo roughly indicated for comprehension purposes.

from the charge balance equation and involves the electric vorticity $W = \nabla_\perp^2 \Phi$, defined under a Boussinesq-like approximation. Together, Eqs. (3) and (4) give the electrostatic potential Φ, and hence the electric field $\mathbf{E} = -\nabla\Phi$.

The electric drift velocity $\mathbf{u}_E = \mathbf{E} \times \mathbf{B}/B^2$ advects mater, current and ion momentum across the magnetic field. $\eta_\parallel$ is the parallel resistivity of the plasma while D, ν and D_Γ are diffusion coefficients, accounting for collisionnal processes. In Eq. (4), the divergence of the diamagnetic current is reduced to a curvature term propotionnal to g. Finally the system is flux-driven, with a density source term S (gaussian shape of radial length L_s and centered on X_s) mimicking an incomming flux from the core.

We only consider the SOL, all magnetic field lines ends at the divertor plates, where Bohm boundary conditions are applied on particle fluxes and currents:

$$\Gamma_{\parallel \mathrm{se}} = \pm N_{\mathrm{se}} \exp(\Lambda - \Phi_{\mathrm{se}}) \qquad J_{\parallel \mathrm{se}} = \pm N_{\mathrm{se}}(1 - \exp(\Lambda - \Phi_{\mathrm{se}}))$$

The *se* subscript is refering to the value of the quantity at the sheath entrance while $\Lambda = \ln(m_i/2\pi m_e)/2$, the normalized sheath potential drop, corresponds to the equilibrium potential which cancels out the sheath current and screens the wall from the plasma. In this paper, simulations are run on a 128x256x32 mesh, for a duration of typically 10^5 time steps with standard parameters of Table 1:

Table 1 Standard values of non-dimentional control parameters used in the 3D simulations.

dt	$L_\parallel$	L_X	L_Y	η	Λ	g	D, D_Γ & ν	S_0	X_s	L_s
1	12.10^3	256	256	10^{-5}	2.8388	3.10^{-3}	10^{-2}	10^{-2}	32	8

For a typical hydrogen discharge, with a magnetic field of B_0= 3T, density around $10^{19}\mathrm{m}^{-3}$ and an electronic temperature equals to 100 eV, the Larmor radius ρ_L= 0.3mm and the simulated plasma takes place in a narrow box of 87mm x 87mm x 8m. *The rather high collisionnality $\eta_\parallel$ = and the length of field lines are then comparable to those of a small tokamak*

2.2 Synthetic probes models

The layout of the problem is illustrated in Fig. 1. In a first part, a biased probe is inserted in the center of the top divertor plate at $Z_\mathrm{p} = L_\parallel$. For the second part, the body of a swept probe is plunged into the SOL plasma, either at one-half of one-fourth of the field lines, ie. $Z_\mathrm{p} = L_\parallel/2$ or $Z_\mathrm{p} = L_\parallel/4$.

The interaction between the probe and the SOL plasma is described by the sheath theory in strong magnetic fields, with field lines perpendicular to the wall [4]. The flushed probe is then modeled by a local polarization of the target plates, via a modification of the parallel Bohm boundary conditions :

$$\Gamma_{\parallel \mathrm{p}} = \pm N_\mathrm{p} \exp(\Lambda - \Phi_\mathrm{p} + \Phi_{\mathrm{wall}}) \qquad J_{\parallel \mathrm{p}} = \pm N_\mathrm{p}(1 - \exp(\Lambda - \Phi_\mathrm{p} + \Phi_{\mathrm{wall}}))$$

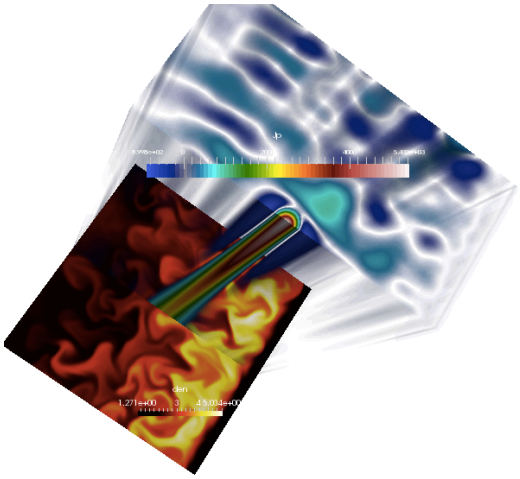

Fig. 2 3D view of $J_{\|}$ from the top, where the probe is located. The white/transparent color indicates zero current. The bottom plan shows the XY density map in strong SOL electrostatic turbulence.

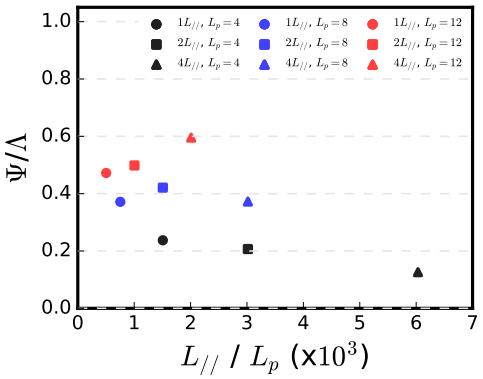

Fig. 3 Amplitude of the perturbation in front of the probe versus the ratio of the parallel to the probe lengths. Circles are for parallel length of 6x10^3, squares and triangles are respectively for twice and fourth times the first $L_{\|}$. Colors show probes of the same sizes.

$\Gamma_{\|\mathrm{p}}$, N_p, Φ_p and $J_{\|\mathrm{p}}$ are plasma quantities in front of the probe but still at the sheath entrance. The wall polarization has a gaussian shape $\Phi_\mathrm{wall} = V_\mathrm{p}\ \exp(-(X-X_\mathrm{p})^2/L_\mathrm{p}^2)\ \exp(-(Y-Y_\mathrm{p})^2/L_\mathrm{p}^2)$ with V_p the applied bias voltage, $(X_\mathrm{p}, Y_\mathrm{p})$ the position and L_p the size of the probe. In the limit of strong negative polarization[1], the Boltzmann exponential term tend toward zero locally: only ions reach the probe and the current drawn by the probe is equal to the ion flux, ie. the probe is run on ion saturation mode.

On the other hand, the probe body is geometrically modelled by introducting a solid obstacle with sheath boundary condition in the middle of the plasma. The probe covers an area of 32 ρ_L in the poloidal direction and occupies radially the second half of the computationnal zone. In the parallel direction the probe is infinitly thin, which seems reasonnable when considering the size of the probe in comparison to the parallel length $L_{\|}$ of the plasma. At least, the probe body is taken conductive, but could just as well be chosen insulating, as we will mostly focus on density and flux perturbations.

3 Polarisation of the divertor probe

As stated in previous works [21–23], the Langmuir probe in ion saturation mode impacts the surrounding plasma and could give measurements leading to an underestimation of the plasma quantities. An illustration of the perturbation is given in Fig. 2 : the parallel current drawn by the probe is maximum at the front of the probe, decreasing along and spreading across the magnetic field lines. We can also observe close to the probe the area of the return current which extends non-symetricaly along the radial direction on approximately one probe size L_p. Following the Ohms law Eq. (3), the parallel current has to come from a parallel gradient of potential and thus requires that the plasma in front of the probe stays at a different potential than the one of the unperturbed plasma. The perpendicular electric field which rises then gives birth to an ExB vortex around all the flux tube, preventing the turbulent plasma to reach the probe tip. To study this phenomon, we define $\Psi = \Lambda - \Phi_\mathrm{p}$, the difference of potential between the front of the probe and the unperturbed plasma, which characterizes the magnitude of the perturbation and thus the strengh of the vortex. We also look at $l_{\|}$, the parallel extention of the perturbation.

In a semi-infinite plasma, the perturbation would extend along the field lines until the current transported across the magnetic field compensates the current drawn by the probe $J_{\|\mathrm{p}} = l_{\|}\nabla_\perp \cdot \mathbf{J}_\perp$. Considering the turbulent perpendicular transport of current around the probe as an hyper-diffusif process $\mathbf{J}_\perp = -\nu_\mathrm{turb}\nabla\nabla^2\Phi$ of

[1] with a typical SOL electronic temperature $T_0 \approx 100$ eV, $V_\mathrm{p} = -3$ corresponds to approximately -300V

perpendicular scale L_p, and combining this with Eq. (3), the parallel scale $l_\parallel$ of the perturbation can be estimated as :

$$l_\parallel = \sqrt{\frac{\eta^{-1}}{\nu_\mathrm{turb}}} L_\mathrm{p}^2 \tag{5}$$

Then, the integration of the current divergence equation along the parallel direction from the probe to $l_\parallel$ where the perturbation vanish and no parallel current exists let us express the amplitude of the perturbation as :

$$\Psi \approx \sqrt{\frac{\eta}{\nu_\mathrm{turb}}} L_\mathrm{p}^2 = l_\parallel \eta \tag{6}$$

Fig. 3 shows the amplitude of the perturbation normalized to the floating potential as a function of the ratio $L_\parallel / L_\mathrm{p}$. There is two immediate observations : the first one is that Ψ does depend on the parallel length of the domain $L_\parallel$, in contradiction with the simple semi-infinite plasma assumption, where the perturbation should vanish at $l_\parallel \ll L_\parallel$. The second observation, which accords well to Eq. (6), is that at a fixed $L_\parallel$, a larger probe will produce a larger perturbation.

On another hand, we could have expected that increasing the parallel length would lead to weaken the perturbation as the perpendicular current would have been collected on a longer area. This is correct for the small probe L_p=4, but in contradiction with the results of the simulations for probes of size L_p=8 and L_p=12. This difference can however be explained when reconsidering the semi-infinite plasma hypothesys : as a matter of a fact, the SOL plasma takes its place between the two sides of the limiter/divertor separated in our simulations by a parallel length of 6x10^3 - 2x10^4 (hence around 5m-20m, in a small tokamak with $T_e^{(\mathrm{SOL})} \approx$100eV). With a parallel resistivity η of 10^{-5}, the parallel scale of the perturbation is of the same order or even exceed the parallel length of the system : $l_\parallel / L_\parallel \in$ [1,10]. The perturbaton reaches thus easily the opposite wall, drawing current directly from it. In this case, the probe IV characteristics should be interpreted as those of double probes.

Supposing now that the total perpendicular current divergence is low enough (with a very short parallel length for example) to consider $\nabla_\parallel \cdot \mathbf{j} = 0$ giving a parallel current constant all along the field line and equal to the saturation current drawn by the probe. Inserting in Eq. (3) then gives :

$$j_\parallel = -\eta^{-1} \nabla_\parallel \Phi = j_\mathrm{sat} \qquad \text{and thus} \qquad \Phi_\mathrm{opp} - \Phi_\mathrm{p} = L_\parallel \eta j_\mathrm{sat} \tag{7}$$

Moreover, as no curent comes from the perpenducular direction, the current drawn by the probe has to come entirely from the opposite wall. Expressing Φ_opp with the sheath theory and substituting the saturation currents, we can see that when the perpendicular current divergence is weak :

$$\Psi = \ln\left(1 + \frac{N_\mathrm{p}}{N_\mathrm{opp}}\right) + L_\parallel \eta N_\mathrm{p} \tag{8}$$

In this situation, the perturbation in front of the probe grows when $L_\parallel$ increases. For a given probe size, two behaviours are then in competition depending on the total divergence of the perpendicular current, and there is a maximum of the amplitude of the perturbation at a specific $L_\parallel$, which can be seen on Fig. 3 for the L_p=8 probe size.

Another way to look at Ψ, remember of Stangeby [19], is considering it as an adaptation to the probe voltage : indeed, rewriting the definition of Ψ as $\Phi_\mathrm{p} = \Lambda - \Psi = \Lambda - \alpha V_\mathrm{p}$ let us define $\alpha = \Psi / V_\mathrm{p}$, an accomodation factor of the plasma potential to the probe voltage, positive and even between zero and one. Then in sweeping operations to measure IV characteristics, if the plasma potential adapts to the probe voltage, the elecron current drawn by the probe should also be affected :

$$J_{\parallel\mathrm{p}}^e = N_\mathrm{p} \exp\left(\Lambda - \Phi_\mathrm{p} + V_\mathrm{p}\right) = N_\mathrm{p} \exp\left(V_\mathrm{p}(1-\alpha)\right) \tag{9}$$

As a consequence, we see that if α differs significantly from zero, the measured slope on the IV characteristic, T_e, will always be overestimated, by the factor $(1-\alpha)^{-1}$.

Let us look now at the effect of η on the perturbation. When the probe is run in ion saturation mode, we are mostly interested by the density perturbation just in front of it. Eqs. (5), (6) and (8) tell that increasing the

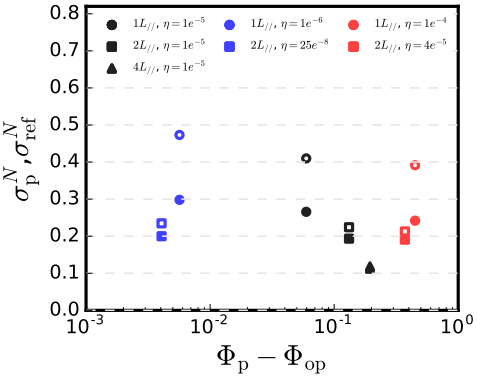

Fig. 4 Standard deviations of density fluctuations in front of the probe (filled symbols) in comparison with the reference case (empty symbols) as a function of the potential difference between the walls. In blue on the left (small electric field), are the "conductive" cases with a low η. On the right (high electric field) are the "resistive" cases. Circles, squares and triangle are respectively for the base parallel length, times two and four.

resistivity should lead to a stronger perturbation, with a lower parallel extension. Also, when $l_{\|}$ is small enough, we can expect the transport barrier created by the vortex to act only on a part of the field line, and consequently that it exists a plasma refilling of the probe channel by parallel transport from the other side of the flux tube. On the contrary, if $l_{\|}$ is long in comparison to $L_{\|}$, the perturbation should be constant along the field line, reaching the opposite wall, and the vortex would prevent the plasma to enter the probe channel from either sides. Less obvious on the mean plasma density, this effect is clear on the fluctuations levels, as showed on Fig. 4, from which we can extract two main trends :

1. Fluctuations are largely reduced in comparison to the unperturbed case, when the parallel length $L_{\|}$ is small, which is less evident when increasing the resistivity.

2. Increasing the resistivity leads to a small reduction of σ_N and σ_{ref}, but the principal effect is the increase of the parallel electric field.

In the case of ITER, where the plasma will be hot and highly conductive, we can expect a strong connection of the perturbation between the two sides of the divertor. The flushed mounted probes should then act like double probes, the current being limited by the sheath of the opposite wall.

These results should nethertheless be significantly impacted by the plasma-neutrals interactions short-circuiting transverse transport of current and by the shear of the magnetic field impacing the shape of the probe flux tube.

4 Reciprocating probe body and synthetic Mach measurements

In this section, we study for the first time the impact of a probe body inserted in the SOL plasma with a full 3D turbulent code, at the scale of the Larmor radius. The geometry and the dimensions of the problem are sketched on Fig. 1 of the model section. After a description of the main impacts of the probe on the SOL plasma characteristics, we will reconstruct and study a synthetic Mach probe measurement following the Hutchinson theory [8].

4.1 Perturbation the SOL plasma due to the probe body

The first principal effect of the insertion into the SOL of a solid object is the creation of its own secondary pre-sheaths, the object's shadow [12]. Indeed, as the length of the field lines is divided by two and the loss surface for the plasma doubles, it will exist, on the both side of the probe, two areas of reduced density, where the radial decay length is strongly shortened. This effect is clearly recovered in the simulations, as we can see on the Figs. 5 : the shadow of the probe extends along all the field lines, the plasma density is depleted in the probe shadow, from 20% to more than 40%, and this just few ρ_L after the first contact between the plasma and the probe. The plasma potential, which responds to the plasma pressure accordingly to the Boltzmann relation, is also deeply impacted : the potential difference which emerges between the unperturbed plasma and the probe shadow gives birth to perpendicular electric fields, radials along the borders of the probe and poloidal in front of

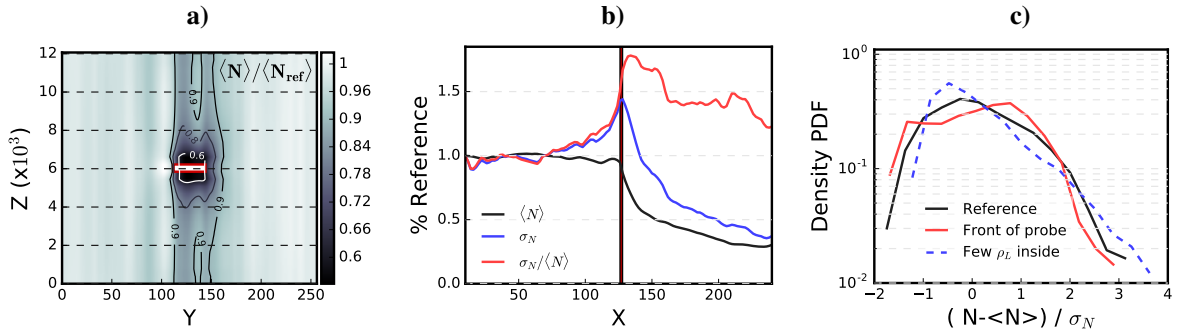

Fig. 5 **a)** Probe shadow in the poloidal plane. Map of the mean plasma density in comparison with the unperturbed case around the probe. The probe, in white, is situated at the middle of the field lines. **b)** Radial profile of the mean density, standard deviations and standard deviation normalized to $\langle N \rangle$, rapported to the unperturbed reference case. The black line denotes the contact point with the probe. **c)** PDFs of density for the reference case, just in front of the probe and few Larmor radius inside the probe shadow.

it. As in the flushed probe cases, this perpendicular electric field creates strong transport barriers all around the shadow, accentuating the plasma depletion.

These two effects, namely the dump of plasma density due to presence of the probe and the transport barriers, both impact the plasma fluctuations inside the probe shadow, either by "reducing" the frequency of bursts and also by increasing their relative importance in comparison to $\langle N \rangle$. In front of the probe, where the poloidal transport barrier emerges, the PDF shows that there is much more middle or mixed events, corresponding to avalanches stopped and redirected. More inside the probe shadow, we clearly observe a modification of the kurtosis of the PDF indicating less frequent but more important events. They correspond to the avalanches which pass through the barrier, with a density relatively much more important than the plasma in the probe shadow.

In this simple case, without parallel or poloidal mean flows, it should be

4.2 Synthetic Mach measurements

Measurements of plasma flow velocity are of prime importance in tokamaks and so far, Mach probes, or so called "Janus" probes, are the principal diagostics used in this objective. The principle of these probes is to measure the ion fluxes parallel to the magnetic field on both sides of the probe, the ratio of the fluxes giving then the Mach number of the flow. The theory, a one-dimentional model first developped by Stangeby [9] and refined by Hutchinson [10–12], is based on the following equations :

$$\nabla_{\parallel} \Gamma = -\nabla_{\perp} \cdot (N \mathbf{V}_{\perp}) \tag{10}$$

$$\nabla_{\parallel} \left(\Gamma^2 / N \right) + 2 \nabla_{\parallel} N = -\nabla_{\perp} \cdot (\Gamma \mathbf{V}_{\perp}) + \eta_H \nabla_{\perp}^2 M \tag{11}$$

with the symbols defined according to (1)-(4), $\mathbf{V}_{\perp}$ being the normalized perpendicular velocity, $M = \Gamma / N$ the parallel velocity normalized by the Bohm velocity, *i.e.* the Mach number and η_H, the shear viscosity, introduced by Hutchinson, which is the term differencing fundamentaly his model from the one of Stangeby.

The essence of this one-dimentional approximation is to consider the perpendicular divergence of fluxes as sources of matter and momentum :

$$S_N = -\nabla_{\perp} \cdot (N \mathbf{V}_{\perp}) \tag{12}$$

$$S_{\Gamma} = -\nabla_{\perp} \cdot (\Gamma \mathbf{V}_{\perp}) - M \nabla_{\parallel} (NM) + \eta_H \nabla_{\perp}^2 \Gamma / N \tag{13}$$

For the particle source, Stangeby use either $S_N = $ cste. or $S_N \propto N$ while Hutchinson prefers to use a source deriving from a diffusive particle flux $S_N = D_{\perp} \left(N_{\infty} - N \right) / a^2$, with a unperturbed plasma density N_{∞} and a

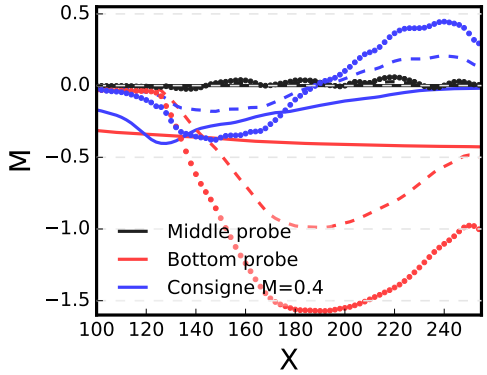

Fig. 6 Synthetic measurement of flow Mach number following both formulas of Stangeby (dotted lines) and Hutchinson (dashed lines) and for three test cases : Black lines for the probe situated in the middle of the computational domain at $Z = L_{\parallel}/2$ with zero imposed parallel flow. Red Lines for a probe positioned at $Z = L_{\parallel}/4$ also without external parallel flow. Blue lines for the probe situated at $Z = L_{\parallel}/2$ but with an M = 0.4 imposed external flow velocity.

the characteric perpendicular length of the probe. About the momentum source, that Hutchinson resumes as [8]:

$$S_\Gamma = \frac{D_\perp}{a^2 c_s}\left(M_\infty - M\right)\left(N_\infty - N\left(1-\alpha\right)\right) \qquad \text{with} \qquad \alpha = \eta_H / N D_\perp \tag{14}$$

$$S_\Gamma = \frac{D_\perp}{a^2 c_s}\left(M_\infty - M\right)\left(N_\infty\left(1+\alpha\right) - N\right) \qquad \text{with} \qquad \alpha = \eta_H / N_\infty D_\perp \tag{15}$$

the inviscid case of Stangeby is recovered with by $\alpha = 0$ and S_Γ reduces to $S_N\left(M_\infty - M\right)$, representing the change in momentum of the flow in the flux tube due to the entrance of ions with the unperturbed velocity M_∞. These two approaches give for Stangeby and Hutchinson respectively the following ratio of upstream to downstream fluxes : $R = (2+M_\infty)/(2-M_\infty)$ and $R = \exp\left(M_\infty/M_c\right)$, the value of the calibration factor M_c, resulting from a fit of models results, being situated between 0.41 (1D model) and 0.45 (2D). Hutchinson also remarks that in their experiment, Harbour and Proudfoot [31] fit this ratio with M_c = 0.6, which could correspond to an α = 0.1 situation.

We reproduce these two measurements in figure 6 for three different cases. The first one, where the probe is situated at the middle of the domain and without any parallel flow, measure the same density on each side of the probe (as the geometry is symmetric) and thus a correct parallel flow of M_∞ = 0 for the both models. In the second case, where the probe is situated at the bottom of the computation area, we can see that the measured Mach number, for the two models, varies between 0 and -1.5 along the radial direction. The both measurements give nethertheless the right value of $M_\infty \approx 0.4$ at a radial distance from the probe tip of respectively 6 (Stangeby) and 15 (Hutchinson with M_c = 0.45). In the third case, the probe is back to the center of the field lines, but we impose an external flow Mach number M_∞ = 0.4 at the probe tip. Again, both measurements depends on the radial positition, but as the formula given by Stangeby give the right value at $X - X_p$ = 8, the model of Hutchinson underestimate everywhere the flux velocity. At least, the both methods depend on the positioning of the probes on the probe body. If Stangeby's seems more accurate in our model of turbulent perpendicular transport, Hutchinson measurement can be calibrated with M_c. It is then worth to say that M_c should be specific of a probe design and that none value could be used universaly.

Finaly, it should be pointed out that in the case of an uncentered probe, the density difference may not be only due to the probe wake. Indeed, if we modelize the perpendicular transport by a constant diffusion of coefficient $D_\perp$, the presheath equilibrium is reached when :

$$\nabla_\parallel \Gamma = D_\perp \nabla_\perp^2 N \tag{16}$$

resulting in an radial profile exponentialy deacreasing for the density, whose decay length λ_{SOL} defines the size of the SOL :

$$\lambda_{\text{SOL}} = \sqrt{\frac{D_\perp L_\parallel}{c_s}} \tag{17}$$

With a probe separating the SOL presheath of parallel length $L_\parallel$ in two smaller presheaths of different length, saying $L'_\parallel$ and $L''_\parallel$, it is obvsious that the both decay lengths, and thus the density profiles on the two sides of the probes will differ significantly, even when $M_\infty = 0$.

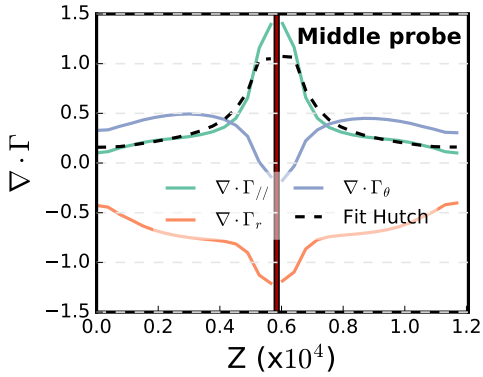

Fig. 7 caption1

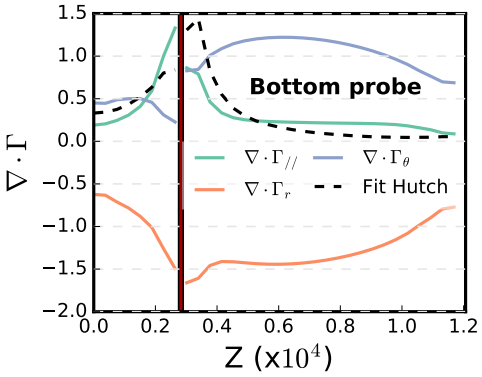

Fig. 8 caption2

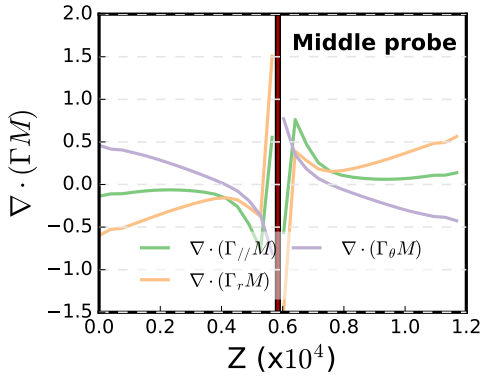

Fig. 9 caption3

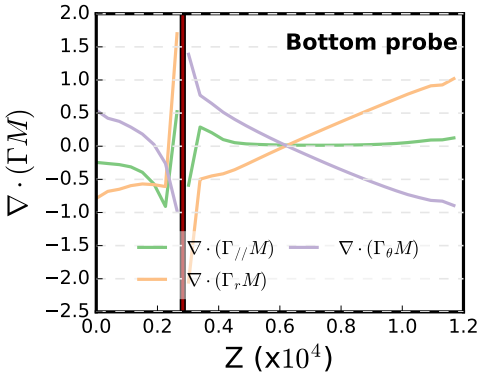

Fig. 10 caption4

5 Conclusion

Acknowledgements This work has been financialy supported by the French National Research Agency through project ANR-11-BS09-023 (SEDIBA). It has been carried out within the framework of the EUROfusion Consortium with a funding from the Euratom research and training programme 2014-2018 in the frame of project WP14-ER-01/CEA-09. The views and opinions expressed herein do not necessarily reflect those of the European Commission. This work was granted access to the HPC resources of Aix-Marseille Université financed by the project Equip@Meso (ANR-10-EQPX-29-01) of the programme "Investissements d'Avenir" supervised by the Agence Nationale pour la Recherche. It also used HPC resources from GENCI-IDRIS in the frame of project i2015056912.

References

[1] I. Langmuir, Journal of the Franklin Institute **196**(6), 751 – 762 (1923).
[2] I. Langmuir, Phys. Rev. **33**(Jun), 954–989 (1929).
[3] L. Tonks and I. Langmuir, Phys. Rev. **34**(Sep), 876–922 (1929).
[4] D. Bohm, Minimum ionic kinetic energy for a stable sheath, 1949.
[5] F. F. Chen, J. D. Evans, W. Zawalski, F. F. Chen, J. D. Evans, and W. Zawalski, Electric probes, in: In Plasma Diagnostic Techniques, edited by Huddlestone, R.H. and Leornard, S.L, (Academic Press, 1965).

[6] G. F. Matthews, Plasma Phys. Control. Fusion **36**(10), 1595 (1994).
[7] P. C. Stangeby, The plasma boundary of magnetic fusion devices, Plasma physics series (Taylor & Francis, New York, 2000).
[8] I. H. Hutchinson, Principles of Plasma Diagnostics, second edition (Cambridge University Press, 2002), Cambridge Books Online.
[9] P. Stangeby, Journal of Nuclear Materials **121**, 36 – 40 (1984).
[10] I. H. Hutchinson, Physics of Fluids **30**(12), 3777–3781 (1987).
[11] I. H. Hutchinson, Phys. Rev. A **37**(Jun), 4358–4366 (1988).
[12] I. H. Hutchinson, Phys. Fluids B **3**(3), 847–856 (1991).
[13] G. F. Matthews and P. C. Strangeby, Journal of Physics D: Applied Physics **22**(5), 644 (1989).
[14] V. A. Rozhansky, A. A. Ushakov, and V. S. P., Nucl. Fusion **39**(5), 613 (1999).
[15] I. H. Hutchinson, Phys. Rev. Lett. **101**(Jul), 035004 (2008).
[16] P. C. Stangeby, Plasma Physics and Controlled Fusion **37**(9), 1031 (1995).
[17] I. H. Hutchinson and L. Patacchini, Plasma Physics and Controlled Fusion **52**(12), 124005 (2010).
[18] R. A. Pitts and P. C. Stangeby, Plasma Physics and Controlled Fusion **32**(13), 1237 (1990).
[19] P. C. Stangeby, Plasma Physics and Controlled Fusion **37**(11), 1337 (1995).
[20] S. J. Zweben, R. J. Maqueda, A. L. Roquemore, C. E. Bush, R. Kaita, R. J. Marsala, Y. Raitses, R. H. Cohen, and D. D. Ryutov, Plasma Physics and Controlled Fusion **51**(10), 105012 (2009).
[21] P. Ghendrih, Y. Sarazin, G. Attuel, S. Benkadda, P. Beyer, G. Falchetto, C. Figarella, X. Garbet, V. Grandgirard, and M. Ottaviani, Nucl. Fusion **43**(10), 1013 (2003).
[22] C. Colin, P. Tamain, P. Ghendrih, F. Schwander, and E. Serre, Contrib. Plasma Phys. **54**(4-6), 543–548 (2014).
[23] R. Futtersack, C. Colin, P. Tamain, G. Ciraolo, P. Ghendrih, Y. Marandet, F. Schwander, and E. Serre, Contributions to Plasma Physics **56**(6-8), 575–580 (2016).
[24] H. M. Mott-Smith and I. Langmuir, Phys. Rev. **28**(Oct), 727–763 (1926).
[25] B. R. Allen J.E. and R. P., Proc. Phys. Soc. **B70** (1957).
[26] B. I.B. and R. I.N., Phys. Fluids **2** (1959).
[27] J. Laframboise, Inst. Aerospace Studies Rept. **100** (June).
[28] K. S. Chung, Plasma Sources Science and Technology **21**(6), 063001 (2012).
[29] A. Paredes, E. Serre, F. Schwander, P. Ghendrih, and P. Tamain, Contributions to Plasma Physics **54**(4-6), 373–377 (2014).
[30] P. Tamain, H. Bufferand, G. Ciraolo, C. Colin, D. Galassi, P. Ghendrih, F. Schwander, and E. Serre, Journal of Computational Physics pp. – (2016).
[31] P. Harbour and G. Proudfoot, Journal of Nuclear Materials **121**, 222 – 228 (1984).